Sample preparation for atomic-resolution STEM at low voltages by FIB

Miroslava Schaffer [a,b,*], Bernhard Schaffer [a,c], Quentin Ramasse [a,b]

[a] SuperSTEM, STFC Daresbury Laboratories, Keckwick Lane, Warrington WA4 4AD, UK
[b] Department of Engineering, George Holt Building, Ashton Street, Liverpool L69 3BX, UK
[c] Kelvin Nanocharacterisation Centre, SUPA School of Physics and Astronomy, University of Glasgow, Glasgow G12 8QQ, Scotland, UK

ABSTRACT

While FIB sample preparation for transmission electron microscopy is a well established technique, few examples exist of samples of sufficient quality for atomic resolution imaging by aberration corrected (scanning) transmission electron microscopy (STEM). In this work we demonstrate the successful preparation of such samples from five different materials and present the refined lift-out preparation technique, which was applied here. Samples with parallel surfaces and a general thickness between 20 and 40 nm over a range of several μm were repeatedly prepared and analyzed by Cs-corrected STEM at 60 and 100 kV. Here, a novel 'wedge pre-milling' step helps to keep the protective surface layers intact during the whole milling process, allowing features close to or at the sample surface to be analyzed without preparation damage. Another example shows the cross-sectional preparation of a working thin film solar cell device to a final thickness of 10 to 20 nm over μm sized areas in the region of interest, enabling atomic resolution imaging and elemental mapping across general grain boundaries without projection artefacts. All sample preparation has been carried out in modern Dual-Beam FIB microscopes capable of low-kV Ga$^+$ ion milling, but without additional preparation steps after the FIB lift-out procedure.

© 2012 Elsevier B.V. All rights reserved.

1. Introduction

Focused ion beam (FIB) microscopy is a well established tool for both imaging and modifying specimens on a micro to nano scale. It has been used in a wide variety of different applications [1]. Its ability to remove material in a highly localized, site specific manner also makes it an ideal sample preparation tool for various other microscopic techniques [2–6] including transmission electron microscopy (TEM). While TEM samples have been prepared with stand-alone ion-beam columns (often called single-beam FIBs) since the 1990s, the widespread use of FIB sample preparation was facilitated by the introduction of dual-beam FIBs, which combine two independent microscope columns, a focused ion beam and an electron beam, in the same machine. The electron column delivers the superior imaging quality of a Scanning Electron Microscope (SEM) and is at the same time less destructive than the FIB imaging. Sample preparation capabilities of FIBs can be further extended by introducing micro-manipulators and gas-injection systems (GIS) into the microscope chamber. The first allows in-situ manipulations such as lift-outs, rotations and transfers of microscopic sample parts during preparation, while the second enables both site-specific material deposition and material-specific preferential milling by introducing reactive gases in the vicinity of the electron or ion probe during operation. Fully-equipped dual-beam FIBs (DB-FIBs) offer great flexibility in TEM sample preparation and many preparation techniques have been developed and reviewed over the years [3,4,7–13]. There are several, often unique, advantages of FIB preparation. The ability to create site specific, cross-sectional samples ('target preparation') makes it an indispensable technique for investigations of modern micro-chips and devices with complicated structure and layout on a sub-micrometer scale. Both surface and buried regions of interest can be accessed and different orientations of the sample (i.e. plan-view or cross-sections) can be achieved using in-situ micromanipulators. FIB's capability to create samples of specific geometry, like thin needles, is especially useful for TEM tomography investigations. The ability to extract small quantities of a material and mount these pieces at fairly exposed positions on dedicated support grids generally helps minimize detrimental bulk-material effects such as charging, magnetic fields or surface migration of contaminants. Finally, FIB sample preparation is generally considered a fairly fast technique, capable of producing a complete sample from a bulk specimen within hours. However, it is sometimes useful to keep in mind that the pursuit of speed often comes at the cost of reduced sample quality.

---

* Corresponding author at: SuperSTEM, STFC Daresbury Laboratories, Keckwick Lane, Warrington WA4 4AD, UK. Tel.: +44 1925 864 902.
  E-mail address: mschaffer@SuperSTEM.org (M. Schaffer).

While FIB sample preparation has been widely used over the last years, serious doubts have appeared on whether the technique is suitable for producing high-quality, ultra-thin specimens needed for modern applications. In particular, two developments in electron microscopy have pushed sample requirements to a new level.

First, the introduction of aberration correction in TEM and scanning TEM (STEM) made directly-interpretable atomic resolution imaging and atomic resolution analytical mapping possible [14–18]. Studies of atomic defects, as well as structural or chemical changes within one or two atomic positions, are now possible and of general interest [19–21]. However, these techniques require very thin, crystalline specimens and are particularly sensitive to structurally damaged material at the surfaces of the TEM sample. There is no doubt that ion beam milling introduces structural damage into specimens, and a certain amount of ion implantation cannot be avoided. The extent of damage is material-dependent and generally increases with increasing ion beam energy. FIB sample preparation tries to minimize this damage by protective surface coating over the area of interest, by milling under a small grazing angle with respect to the sample lamella surfaces, and by using lower energies during the final milling steps. Nevertheless, FIB samples inevitably have a certain amount of damaged surface area, which can prevent high-resolution microscopy depending on its size. Several studies, both theoretical and empirical, tried to explore and minimize the extent of the damaged areas [22–36]. However, because the damage depends on many different parameters that are sometimes hard to control or reproduce, general quantitative conclusion on the minimum achievable damage region has not been reached.

Second, the ability to produce ever more intense electron beams renders issues of electron beam damage more important. Consequently, a trend towards electron microscopy at lower acceleration voltages has emerged, and atomic resolution studies are now carried out in the range of 100 to 40 kV, or even below. With the greatly reduced mean free path of the electrons in the materials (i.e. the mean distance a probing electron travels before interacting with the specimen) at lower voltages, the relative thickness of the observed samples, measured as a fraction of the mean free path (λ), is increased. Suitable specimens therefore have to be much thinner than for high-kV microscopy. It is argued that a relative specimen thickness t/λ between 0.2 and 0.5 is required for very high-end analytical microscopy, resulting in a typical absolute sample thickness between 40 nm and 10 nm for low-kV microscopes. Producing such thin samples that still contain a substantial proportion of undamaged material is a formidable task for FIB milling, and one not easily achieved. However, the present work proposes to show that the current consensus, according to which such a task is generally impossible or at least requires additional ex-situ 'cleaning' steps after FIB preparation, is not justified. Baram and Kaplan [37] have already shown that optimized lamella preparation with 5 kV low-energy milling can produce gold samples of less than 52 nm thickness with sufficient sample quality to allow quantitative atomic-resolution STEM work at 300 kV. Allowing for a wedge-shaped lamella, thinner sample areas may be achieved at the edges [38].

In this work we demonstrate on various material systems that the even higher criteria needed for state-of-the art low-kV microscopy can be met by stand-alone FIB sample preparation using modern dual-beam FIBs offering low-kV ion milling. Using an in-situ lift-out technique with careful adjustments of parameters and procedure, samples, which are as thin as 20 nm or lower over large areas of several micrometers can be prepared without sacrificing the unique advantages of FIB preparation. Using a novel 'wedge pre-milling' step, the protective top layer can be preserved for the final milling steps, allowing for controlled sample preparation of features at or close to the surface, and for very thin samples without a wedge geometry.

2. Methods

2.1. General strategy

Based on the well known standard FIB in-situ lift-out technique [39], we have adapted the procedure following three main strategies: low-kV milling at earlier stages, thick protection layers, and 'wedge pre-milling' to achieve highly parallel lamellas at the final thickness. In addition, extra care has been taken during all other standard preparation steps to avoid all unnecessary ion irradiation and to prevent inhomogeneous milling.

For high-resolution microscopy at low-kV, preventing sample damage at the areas of interest during milling is absolutely key. Hence, estimating the amount of ion beam damage caused in deeper areas by milling the surfaces is needed, and has to be carried out for each different material system. We have used freely available Monte Carlo simulation software (SRIM 2010) [40] to simulate ion-beam interactions with the prepared sample material for various beam energies. The calculations return estimates for ion beam penetration depth and successive atom displacements in the bulk material caused by collision cascades. In particular, for high energies, these cascades extend the 'damaged' area beyond the ion penetration depth. It should be noted, that SRIM does not consider crystallographic information or secondary effects like heat, and hence may well underestimate the true depth of the beam damage. Without being extremely accurate, such simulations can therefore only act as a guide for the FIB thinning process, but they demonstrate clearly why commonly used standard procedures may never achieve suitable thin, undamaged specimens.

To avoid damage in the final lamella, the ion-beam energy has to be progressively lowered during the process down to low-kV milling at the final stage. This must happen sufficiently early, at a much larger thickness than current standard procedures prescribe, so that damage from the previous stage has not already penetrated to the center of the lamella. It should be pointed out that no final in-situ or ex-situ 'cleaning' step can remove damage caused in the interior region due to high energy milling at the earlier stages of the procedure.

It may not be possible to derive an accurate and general 'protocol' of milling steps based on simple beam damage simulations, but the following rule of thumb was successfully used during our work: At any given milling voltage, the minimum thickness was determined by the simulated depth of ion beam damage for the current voltage plus the simulated depth of ion beam damage for all following (lower) voltage milling steps. This thickness was multiplied by two to account for the two milling sides, and then further multiplied by an empirically determined factor between 3 and 5 to account for underestimation of damage by the simulation [32]. It is necessary to stress the point that this rule is only a guide developed with a focus on best quality and not on most efficient sample preparation. Larger safety margins were used to account for changing sample geometry and both milling and thickness measurement imprecision.

To achieve suitably thin lamellas for low-kV microscopy, it is also essential that the sample protection layers stay full intact during the whole procedure including the final thinning. Only then can the final milling steps be performed without introducing inhomogeneities, which generally lead to increased sample damage. We have therefore used substantially thicker protection layers than suggested by the standard procedure.

Due to the tails in the ion-beam profile, milling rates differ between the top and the bottom of a milled lamella, generally

resulting in a preferential thinning of the top (and the protection layers). This effect becomes increasingly prominent the thinner a lamella becomes. We have introduced a novel 'wedge pre-milling' strategy to counteract this problem, such that final lamellas with highly parallel surface can be produced. As this strategy also prevents an early loss of the protection layer, it is also generally key for achieving very thin specimens, in particular if features close to the protection layer (i.e. close to the sample surface of the bulk material) are of interest.

2.2. Instrumentation

Several different FIB systems have been used in the course of this work: An FEI DB-FIB Helios located at Durham University UK, an FEI DB-FIB Nova 200 located at University of Glasgow, an FEI Nova 200 located at University of Leeds, and an FEI DB-FIB Helios as well as an FEI DB-FIB Quanta 3D both located at the Technical University of Denmark in Copenhagen. Naturally, these systems have different configurations and parameters, but with respect to high quality TEM sample preparation the following conditions are generally required.

An in-situ micro-manipulator and a GIS system (for the deposition of a protective layer, typically platinum) are needed for the preparatory steps of the in-situ lift-out technique. To achieve a minimum of surface damage, the availability of low-voltage milling settings with good spatial resolution is paramount. Well aligned and stable settings for a range of voltages and different beam currents are essential to optimize sputter rates during the procedure. In this work, settings for 30 kV, 16 kV, 8 kV, 5 kV, 2 kV, 1 kV, and 0.5 kV were used with varying beam currents and probe sizes for each. High-precision milling of thin lamellas at low voltage also requires a stable sample stage with minimum spatial drift and a highly reproducible and accurate positioning and tilting. Finally, the ion beam scan generator has to offer a sufficient scan resolution to avoid coarse sampling at lower magnification, and different milling procedures or 'scan patterns' have to be available via the software. Using the nomenclature of the FEI software [41], the following three pattern types were used in this work.

The 'rectangle' scanning pattern repeatedly scans the beam over a rectangular array of equally spaced positions using a specified pixel dwell-time. The 'regular cross-section' (RCS) scanning pattern mills a staircase-shaped pattern towards one side of the defined, rectangular area by scanning parts of the area more often than others. The 'cleaning cross-section' (CCS) scanning pattern scans a rectangular area slowly towards one side of the area. This is done by repeatedly scanning one line and shifting this line across the area once. The density of positions in all patterns is defined by the 'overlap' parameter, which calculates the point distances as a relative value of the calculated beam diameter.

2.3. Adapted lift-out procedure

This section describes the preparation steps typically needed for high quality TEM samples. As preparation is highly material-dependent, no universal procedure can be given. The following protocol is thus intended as a set of general guidelines, which highlights important issues. A fair amount of adjustment and user interaction is needed for each individual situation. The aim of this work was to produce thin samples with minimum damage from different materials for high-resolution TEM microscopy at 100 kV or below. Focus was put on sample quality and not on preparation speed or efficiency. Thus, further time-optimized milling procedures may well exist for specific material situations but these are

not dealt with here. Samples were prepared using the following main steps:

1) *Sample pre-treatment.* It is well known that flat, homogeneous and clean sample surfaces reduce artefacts of preferential milling (so-called 'curtaining effect') [3]. Thus, polishing and cleaning the material surface prior to FIB preparation can be beneficial and should be carried out if possible. Next, the sample is coated with carbon by thermal evaporation with a high-quality layer of 30 to 100 nm. This layer provides some initial surface protection and makes the sample conducting. Larger layer thicknesses have the advantage of further reducing curtaining effects during milling. The amorphous carbon layer also provides an excellent area for aberration tuning as needed by the aberration corrected STEM microscopes used during this work. It should be noted that surface coating with metals like Au has been shown to introduce curtaining effects during FIB preparation and should thus be avoided [13]. Standard SEM sample mounting techniques are then used to provide a well conducting bulk sample in the FIB.

2) *Area location and protection layers.* During location of the exact sample position in the FIB, and before protective surface layers have been deposited, the use of the ion-beam should be generally avoided. This is critical if the region close to the surface is of interest. The initial protection layer is deposited with the electron beam with a minimum thickness of 300 to 600 nm. Generally, an electron-beam-deposited-layer is preferable over an ion-beam-deposited-layer as the metal particles forming in the layer are smaller, resulting in smoother milling conditions later. However, due to time constraints, the protection layer can be finished with ion-beam deposition once the initial layer has been deposited. While the deposition of a thick protection layer covering a large specimen area may be time-consuming, it is essential for the preparation of very thin high-quality lamellas. Only then can a sufficient protection layer be kept even during the final milling at sample thicknesses below 30 nm. The total extent of the protection layer should cover the entire area for the lamella preparation (e.g. typically 15×2 μm) and be about 3 μm thick.

3) *Lift-out and transfer.* The in-situ lift-out is performed by the standard procedure [39] and is shown in Fig. 1: Two RCS patterns are used to mill trenches on each side of the lamella. Those trenches are milled sufficiently deep below the area of interested such that ion beam damage of the next milling steps does not affect the region of interest. A U-shaped cut with three 'rectangle' patterns separates the lamella from the bulk, the needle of the micromanipulator is attached with material deposition, and the lamella is cut free with another 'rectangle' pattern. The lamella is transferred to a TEM grid, attached to it by material deposition, and cut free from the needle. Molybdenum grids with a single free standing bar have been used for the samples in this work. The lamella should be mounted both rather at the 'top end' on the bar (Fig. 1d) to minimize redeposition from the grid during FIB milling, and parallel to the TEM grid to avoid the need for high tilting angles during TEM investigation. Finally, the mounted lamella is trimmed to form an even block prior to the actual thinning. Uneven sections at the tip of the lamella, where the needle was attached, may be cut away as well as material sections potentially protruding at the bottom of the lamella. It should be strongly emphasized that during all FIB preparation steps, ion beam illumination of the area of interest should be kept to an absolute minimum, in particular at high voltages, high beam currents and steep incident angles. This becomes increasingly critical for thinner lamellas at later steps. The final mounted lamella has typical dimensions of 1 to 1.5 μm
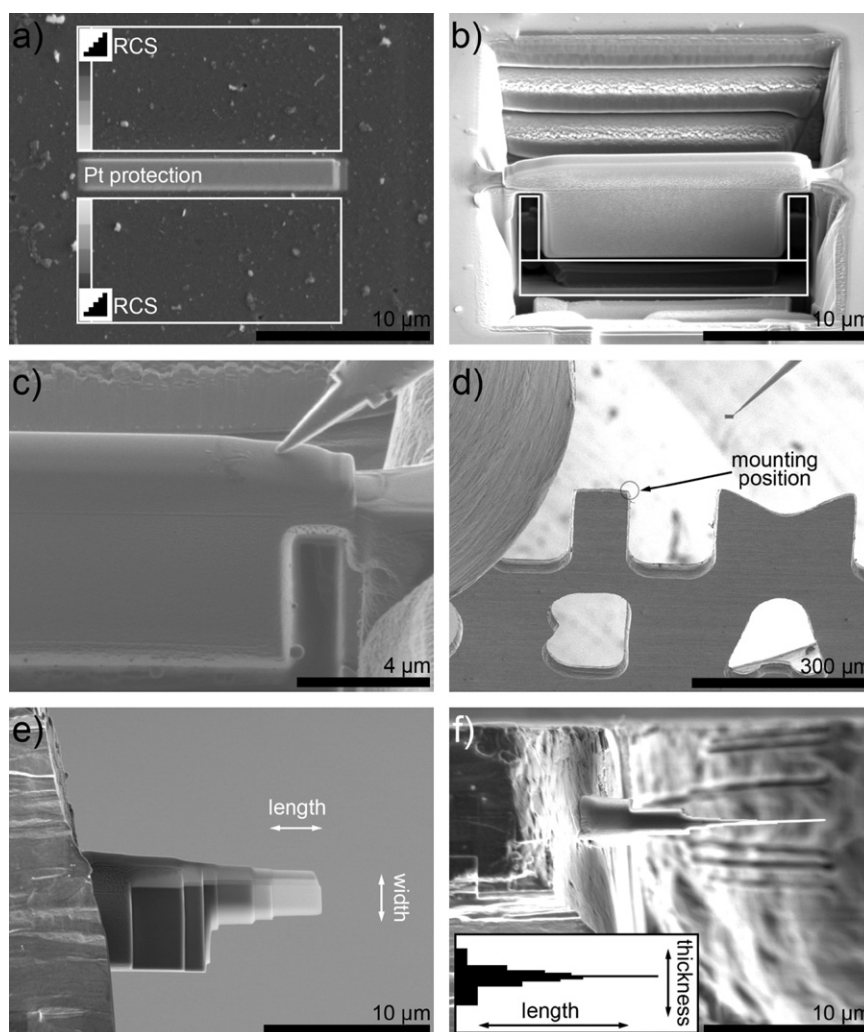
Fig. 1. FIB lift-out technique. a) Deposition of Pt protection layer on bulk surface and position of trench-milling patterns. b) Separation of the lamella from the bulk with U-shaped milling pattern. c) Attaching the micromanipulator tip. d) Lamella transfer to TEM grid with micromanipulator. The arrow indicates mounting position at 'top-end' of bar. e) Lamella on TEM grid at intermediate thinning step. Excess material at lower end has been removed. f) Top view of lamella on TEM grid. Insert shows schematics of 'staircase' thinning.

thickness, several µm of length and a width corresponding to the area under investigation. The surfaces are fairly parallel including the protection layer at the top, which at this stage typically has a remaining width of 2 to 3 µm.

4) *Thinning.* Exact milling parameters, including the thickness values at which the acceleration voltage has to be changed and the sample tilt used during milling, depend on the material system. The values used for the examples shown in this work are summarized in Table 1. As a typical preparation example, the following milling steps have been used for the $NiSi_2/Si$-wafer sample: Rough thinning at 30 kV down to a thickness of about ~1000 nm, followed by 16 kV milling down to ~500 nm, 8 kV milling down to ~200 nm, and 5 kV milling down to ~100 nm. Each of these steps was performed using the CCS pattern and multiple iterations, during which the beam current was varied from high to low. Here, larger currents give faster milling action but less precise milling. In particular during the final steps, lower beam-currents offer sharper probes with less tails, keeping the top protection layers intact until the end. Further low-kV thinning is then performed with the 'rectangle' pattern and a less parallel sample tilt of 4 to 10°. Using the 2 kV setting, the sample was milled down to ~50 nm thickness, and the 1 kV setting was used for the final milling.

In addition to the general procedure just outlined, the following points should be considered during the milling to achieve high-quality results:

- A novel '*wedge pre-milling*' is used during coarse milling (see Fig. 2): While the sample is still thicker than ~1.2 µm, higher tilts of 4 to 7° are used during milling to produce a wedge with a thinner (but still > 150 nm)bottom. Then, while getting thinner, the sides are increasingly made parallel using image contrast as a visual guide. Approximately parallel surfaces should be reached before the 5 kV milling step. This 'wedge pre-milling' helps to reduce redeposition, generally improves the milling performance, and – most importantly – keeps the protection layer intact and an integral part of the parallel lamella when it becomes thin. 'Wedge pre-milling' is especially important for specimens with features close to or at the top of the lamella, when the protection layer must not be destroyed during thinning to final thickness.
- The same milling steps with unchanged parameters are always repeated on both sides of the lamella before changing to the next setting of beam current or voltage. If stage accuracy allows it, the sample is rotated for those steps so that the currently 'milled' surface can be seen with the electron beam.

Table 1
Sample preparation parameters of shown FIB lamellas.

NiSi$_2$ on Si		NiSi$_2$ on Si, backside preparation	
Down to[a]	Parameters[b]	Down to[a]	Parameters[b]
1500 nm	30 kV, $\pm$7°, CCS, 0.5 nA, 0.28 nA	1500 nm	30 kV, $\pm$5°, CCS, 0.5 nA, 0.28 nA
1000 nm	30 kV, $\pm$4°, CCS, 96 pA, 48 pA	1000 nm	30 kV, $\pm$3°, CCS, 96 pA, 48 pA
500 nm	16 kV, $\pm$1.5°–2°, CCS, 45 pA, 21 pA	500 nm	16 kV, $\pm$1.5°–2°, CCS, 45 pA, 21 pA
200 nm	8 kV, $\pm$1.0°–1.5°, CCS, 21 pA	200 nm	8 kV, $\pm$1°–2°, CCS, 21 pA
100 nm	5 kV, $\pm$1°–2.5°, CCS, 16 pA, 8 pA	100 nm	5 kV, $\pm$1°–2.5°, CCS, 47 pA, 16 pA, 7 pA
50 nm	2 kV, $\pm$7°, rectangle, 10 pA	50 nm	2 kV, $\pm$7°, rectangle, 10 pA
Final	1 kV, $\pm$7°, rectangle, 14 pA	Final	1 kV, $\pm$7°, rectangle, 14 pA

NiSi$_2$+Al on Si		CrSi$_2$ on Si	
Down to[a]	Parameters[b]	Down to[a]	Parameters[b]
1200 nm	30 kV, $\pm$5°, CCS, 0.5 nA, 0.28 nA	1400 nm	30 kV, $\pm$7°, CCS, 0.5 nA, 0.28 nA
700 nm	30 kV, $\pm$3°, CCS, 96 pA	800 nm	30 kV, $\pm$4°, CCS, 96 pA,
400 nm	8 kV, $\pm$1.5°, CCS, 62 pA	500 nm	16 kV, $\pm$2°, CCS, 45 pA
200 nm	8 kV, $\pm$1°–1.5°, CCS, 21 pA	250 nm	8 kV, $\pm$1.0°–1.5°, CCS, 21 pA
100 nm	5 kV, $\pm$1°–2.5°, CCS, 47 pA, 16 pA	100 nm	5 kV, $\pm$1°–2°, CCS, 47 pA, 16 pA, 10 pA
Final	2 kV, $\pm$5°, rectangle, 10 pA	50 nm	2 kV, $\pm$2°, CCS, 10 pA
		40 nm	2 kV, $\pm$7°, rectangle, 10 pA
		Final	1 kV, $\pm$7°, rectangle, 14 pA

Thin film solar-cell		YAG-bicrystal	
Down to[a]	Parameters[b]	Down to[a]	Parameters[b]
2000 nm	30 kV, $\pm$4°, CCS, 0.5 nA, 0.28 nA	1500 nm	30 kV, $\pm$4°, CCS, 0.5 nA, 0.28 nA
1000 nm	16 kV, $\pm$2°, CCS, 0.2 nA, 0.13 nA	1000 nm	16 kV, $\pm$3°, CCS, 0.24 nA, 0.13 nA
800 nm	16 kV, $\pm$1.5°, CCS, 45 pA	800 nm	16 kV, $\pm$1.5°, CCS, 45 pA
500 nm	8 kV, $\pm$1°–1.5°, CCS, 62 pA	250 nm	8 kV, $\pm$1°–2°, CCS, 62 pA
100 nm	5 kV, $\pm$1°–4°, CCS, 47 pA, 16 pA	150 nm	5 kV, $\pm$1°–3°, CCS, 47 pA, 16 pA
60 nm	2 kV, $\pm$7°, rectangle, 10 pA	100 nm	5 kV, $\pm$7°, rectangle, 16 pA
Final	1 kV, $\pm$7°, rectangle, 14 pA	60 nm	2 kV, $\pm$7°, rectangle, 10 pA
Final	0.5 kV, $\pm$7°, rectangle, 15 pA	Final	1 kV, $\pm$7°, rectangle, 14 pA

[a] Thickness values are rough estimates by FIB imaging only.
[b] Ion beam high tension, relative tilt, scanning pattern type, ion beam current(s).
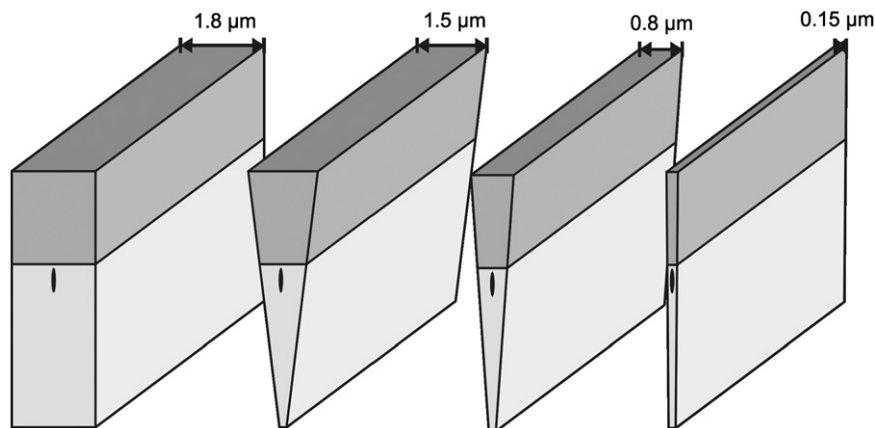
Fig. 2. Schematics of wedge pre-milling. Features of interest close or at the top surface (black ellipse) stay fully protected and protection layers are kept intact and parallel for final thinning steps.

- Long lamellas may also be thinned in staircase shaped steps with only the far reaching end of the lamella being milled to final thickness. However, if such staircase thinning is used, milling patterns on each side of the lamella should be shifted by a small amount with respect to each other for higher stability (Fig. 1f).
- Generally, short dwell times and large beam overlap produce smoother milling, in particular for materials with high sputter rates.
- Ensure that the FIB beam for all used energies is well aligned. In particular at lower voltages, beam profiles

generally degrade and both imaging and milling action are blurred. A best possible beam alignment for low-kV milling is mandatory for high quality preparation results.

- In very stable and well aligned systems, low-kV settings below 5 kV may also be used for the CCS milling provided the beam diameter is small and sharply defined. As CCS milling is performed with small tilts with the beam nearly parallel to the lamella, this has the advantage of less ion beam damage in the final sample as well as more homogeneous thickness. However, this technique carries the danger of completely destroying the sample if a mistake

is made. Using low beam currents and thus slower milling minimizes this risk.

5) *Finalizing and transfer.* Once the lamella has been prepared to the final thickness, the electron beam is turned off and ion milling at both sides is briefly repeated with the last set of parameters. This cleans off the contamination layer introduced by the electron beam imaging. Depending on the sample material and lamella thickness, the sample may need storage under protective atmosphere or vacuum, as surface reaction layers such as native oxides may play an increasingly strong role.

Samples in this work were all prepared following the adjusted lift-out technique described above. They were then stored under vacuum and no other sample treatment other than a 4 h bake at about $6.0 \ 10e-6$ Torr, was applied prior to the STEM investigation. All STEM-results were acquired using the aberration corrected NION UltraSTEM 100 microscope at SuperSTEM Laboratory Daresbury/UK. This is equipped with a Gatan ENFINA spectrometer for electron energy-loss spectroscopy (EELS). Beam convergence semi-angle alpha and EELS collection semi-angle beta during shown measurements were 30 mrad and 31 mrad, respectively.

3. Results

The focus of this publication is to demonstrate by various examples the general suitability of FIB preparation for high-resolution STEM imaging and EELS analysis at low voltages. Samples of several material systems were prepared during the course of different investigations. Results and sample particulars of these investigations, which are not relevant to the scope of this publication, have been and will be published separately.

The first set of samples was prepared to study the interfaces and structure of metal-disilicide thin films on silicon. As the features of interest lie within the first 50 nm from the surface, special care was taken to protect this region even through final milling using the 'wedge pre-milling' outlined before. A $NiSi_2$ thin film on Si-wafer material was chosen as the first test system for optimized FIB preparation and three samples were prepared with slight variations of the preparation procedure with respect to pixel dwell-time, scan position overlap and beam current. While all samples showed specimen thickness below 40 nm over a large and homogeneous area of several µm, the best results were achieved using the parameters given in Table 1. Fig. 3a shows the STEM bright field (BF) image of a part of the lamella. Sample thickness shown in the insert was measured as relative thickness by EELS, assuming an inelastic mean free path λ of 72 nm (Si, 100 kV). Despite a general thickness of only 20–25 nm in the Si wafer, the sample showed no bending contours over its whole length and is homogeneously thin over the entire area. Surface protection layers (carbon and e-beam deposited Pt/C) were fully intact. HAADF high-resolution images of the [110] oriented Si wafer (not shown) displayed clearly resolved Si-dumbbells without contrast variations of the background, indicating clean and homogenous sample surfaces. However, the $NiSi_2$ to Si interface showed a several nm broad band of diffuse
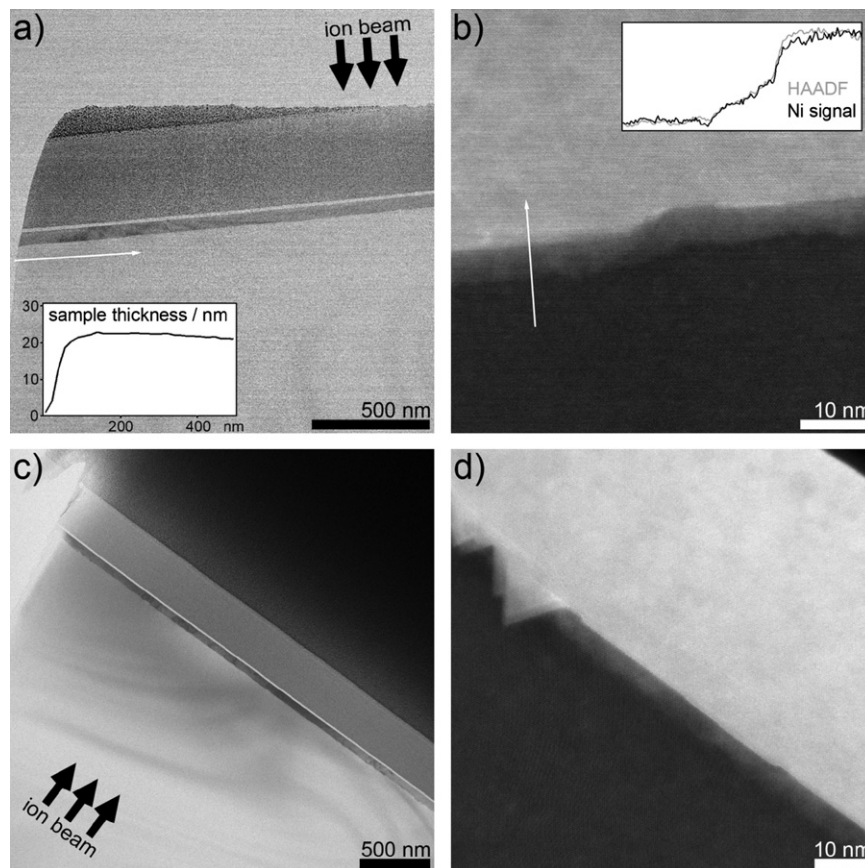
Fig. 3. $NiSi_2$ layer on Si-wafer, prepared by FIB. a) Low magnification STEM BF image showing no bending contours and homogeneous thickness over a large area. The insert shows the specimen thickness measured by EELS from the line scan indicated by the white arrow. Black arrows give the direction of the ion-beam during FIB milling. b) Medium magnification STEM HAADF image of the $NiSi_2$/Si interface. Diffuse contrast at the interface corresponds to the nickel content as shown by EELS line scan from the indicated white arrow (insert). c) Low magnification STEM BF image of 2nd lamella prepared by backside technique. Black arrows indicate the direction of the ion-beam during FIB milling. d) Medium magnification STEM HAADF images of the interface of the 2nd lamella showing both the diffuse interface and pyramid features.
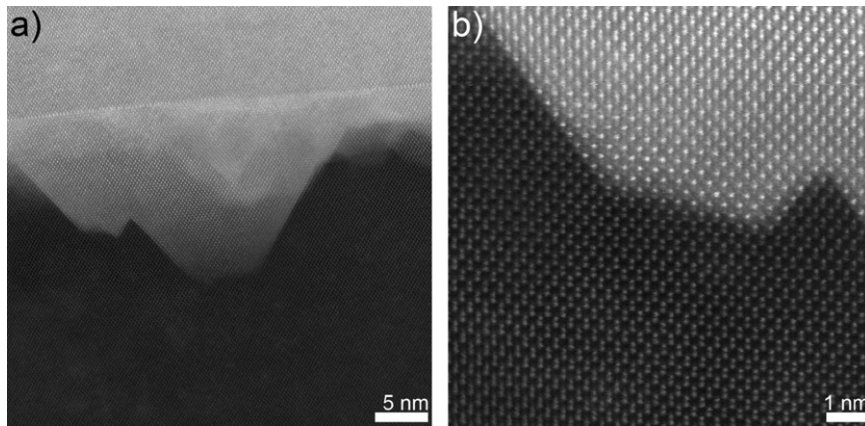
Fig. 4. High magnification STEM HAADF images of the pyramid features found in backside prepared $NiSi_2$/Si lamella. The features show sharp interfaces but the projection of features can appear as diffuse interface layer.
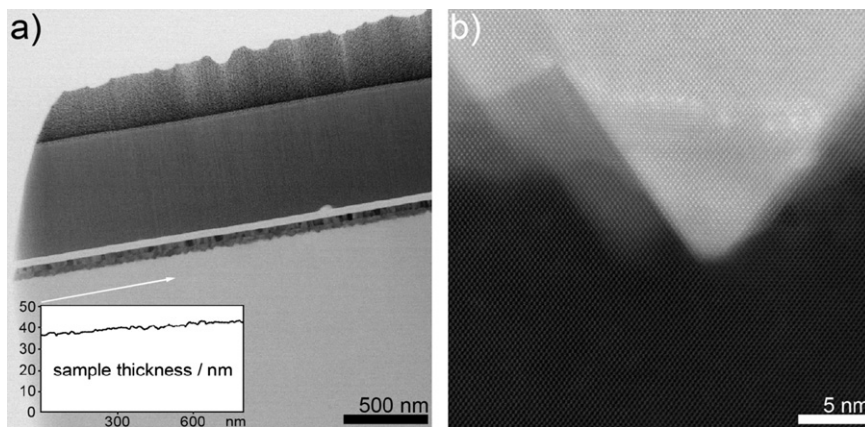
Fig. 5. $Al+NiSi_2$ layers on Si-wafer, prepared by FIB. a) Low magnification STEM BF image showing that a double-layer has formed. Insert shows measured sample thickness by EELS line scan as indicated by the white arrow. b) High magnification STEM HAADF image showing pyramid structures at the interface to the Si wafer in [110] orientation.

contrast (Fig. 3b), which was initially not expected. An EELS line scan yielding a Ni elemental profile with simultaneous HAADF signal across this layer verified that the contrast is due to increased nickel content whereas no Ga could be detected above the EELS detection limits. At this stage, artefacts due to the FIB preparation could not be excluded. A 4th FIB lamella was thus prepared from the same material using a 'backside' preparation technique [11,42]. Here, a large block of the original sample material is extracted from the bulk by FIB lift-out and mounted to the grid after a 180° rotation in a two-step procedure. The milling direction during TEM lamella thinning is thus reversed, as indicated by the black arrows in Fig. 3a and c. This new lamella showed identical 'blurred' interfaces as the first (Fig. 3d). Furthermore, other sections of the sample clearly dispayed pyramid-shaped interface structures in the 1 to 20 nm size range. These features showed atomically sharp interfaces to the Si wafer (Fig. 4). It can thus be concluded that the observed interface contrast is not a FIB preparation artefact, but a projection of the real interface structure of the $NiSi_2$ layer in this sample. A second specimen of this study, a Ni/Al metal-disilicide layer on Si-wafer, showed similar interface structure (Fig. 5). It should be noted that due to the dimensions of the features (2–20 nm basal length), thin samples are also required for (S)TEM work at higher voltages than 100 kV to avoid geometric projection.

A FIB lamella of a different material from this study is shown in Fig. 6a. Again a large, straight, and homogeneously thin sample with thickness ~25 nm over a large area was prepared without losing the surface protection layers. The $CrSi_2$ layer of this sample

was not homogeneous in size and was completely missing in several defect areas. Fig. 6b shows a medium magnification BF image of such an area where the $CrSi_2$ is completely missing and several twin-boundaries (TBs) can be found in the silicon. Atomic resolution HAADF images of the $CrSi_2$ (Fig. 6c) and the silicon TB (Fig. 6d) demonstrate the high quality of the FIB sample. The top surface of the sample has been fully protected under the carbon and Pt/C layers, and quantitative analysis can be performed from the HAADF signal intensities.

Another example of successful FIB preparation for low-kV atomic resolution STEM investigations is shown in Fig. 7. Here, a near $\Sigma5$ grain boundary in an yttrium aluminum garnet (YAG) bi-crystal was studied by EELS at both 100 kV and 60 kV to understand diffusion mechanisms. Following the preparation as described in Table 1, a specimen of below 30 nm thickness could be prepared of the interface area, as measured by an EELS line scan from the indicated area. Due to the need for target preparation and the thickness requirements of low-concentration elemental analysis, previous preparations – both FIB and non-FIB – proved to be insufficient. This FIB sample enabled the intended experiment for the first time, and made it possible to further reduce the acceleration voltage to 60 kV (earlier studies had been carried out at 300 kV and 100 kV), thus minimizing sample damage on a notoriously sensitive garnet. Further results are published elsewhere [43].

The final example shows one of two prepared FIB cross-sections of a working thin film solar cell. This device was grown
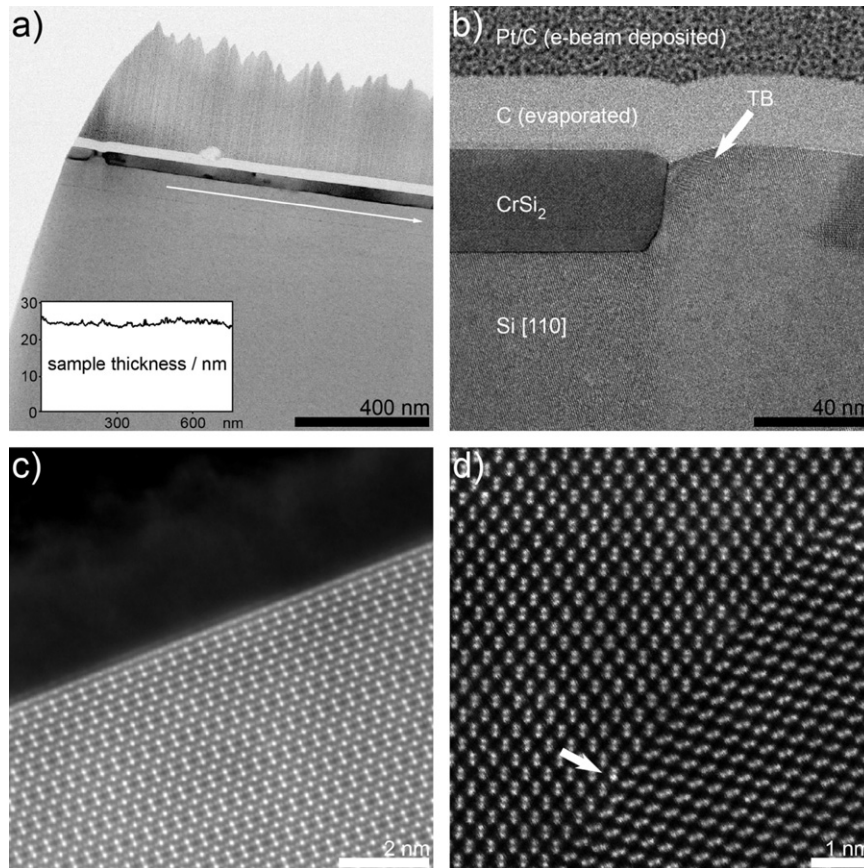
Fig. 6. $CrSi_2$ layer on Si-wafer, prepared by FIB. a) Low magnification STEM BF image showing the general sample quality. The insert shows the measured sample thickness of an EELS line scan as indicated by the white arrow. b) Medium magnification STEM BF image showing a region of missing $CrSi_2$ layer. The Si in this area is twinned several times. c) High magnification STEM HAADF image of the top surface, showing no visible damage of the $CrSi_2$ layer due to FIB preparation. d) High magnification STEM HAADF image of the Si twin boundary as indicated in (b). Z-contrast of individual columns (white arrow) indicates heavier atoms on Si lattice positions.
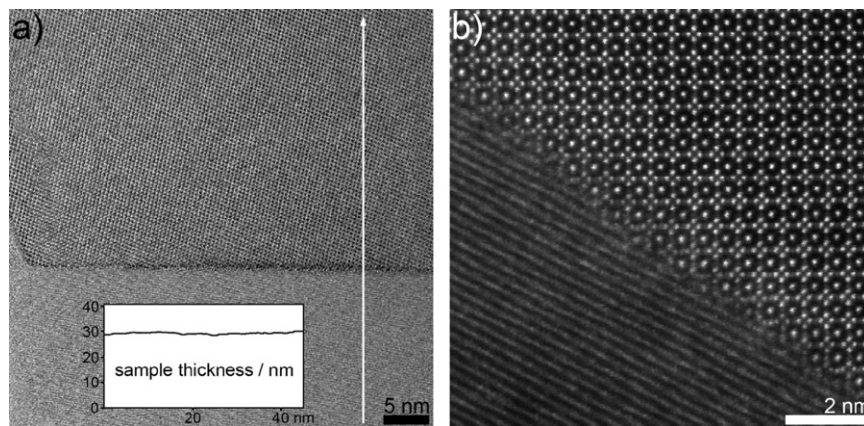
Fig. 7. Medium magnification STEM BF (a) and high magnification STEM HAADF (b) image of the interface in a YAG-bicrystal prepared by FIB target preparation. The insert in (a) shows the measured sample thickness from an EELS line scan indicated by the white arrow.

on a Mo/glass substrate (back contact) and consists of 2 μm thick, polycrystalline Cu(In,Ga)Se$_2$ absorber layer, followed by an about 50 nm thick CdS layer and an about 500 nm thick ZnO layer (front contact) on top. It is well established that the efficiency of these solar cells is influenced considerably by grain boundaries in the Cu(In,Ga)Se$_2$ absorber. However, atomically-resolved compositional analyses of general grain boundaries in working devices have hitherto not been achieved by electron microscopy and EELS.

FIB sample preparation is especially challenging for these specific solar cells. Samples need to be extremely thin even for high-kV investigations, as the geometric projections of the general grain boundaries need to be minimized. At the same time, the rather large grain size requires large sample areas such that a sufficiently large number of grain boundaries can be analyzed. Finally, the sample was prepared as a cross-section of a working device, which exhibits high surface roughness and layers of different sputter rates. As a result, preferential milling is strongly emphasized and can easily lead to preparation artefacts like curtain effects.

The problem becomes increasingly troublesome for thin specimens. Fig. 8a shows the simultaneously acquired image of the high-angle (HAADF) and medium-angle annular dark-field
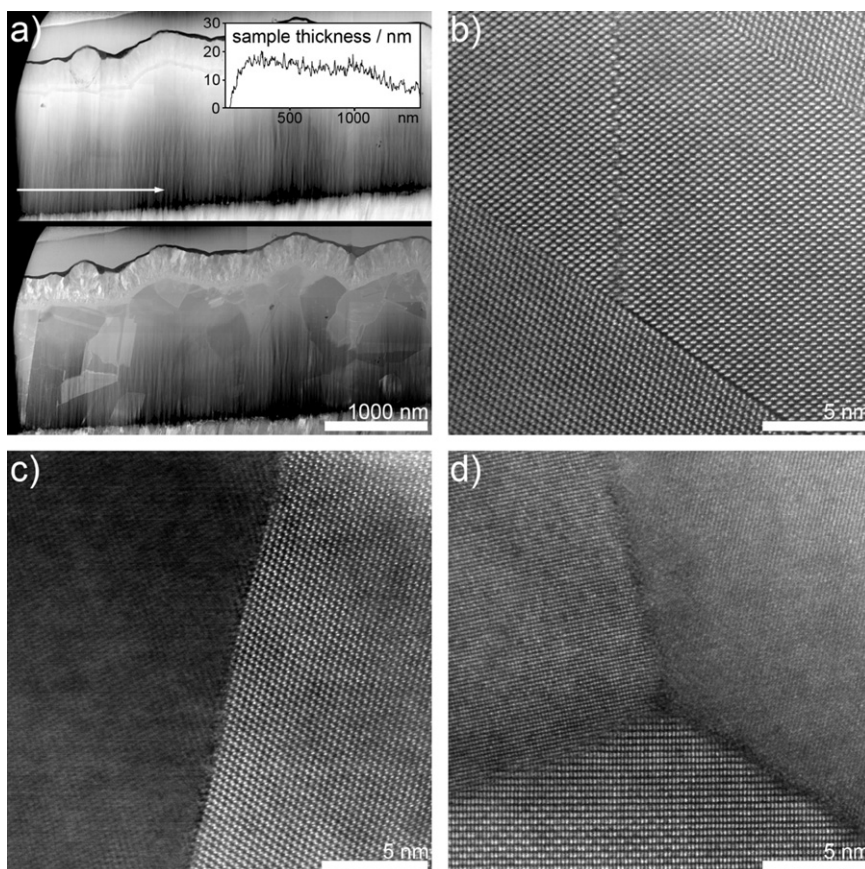
Fig. 8. FIB prepared cross-section of a working thin film solar-cell device. a) Low magnification STEM HAADF (top) and MAADF (bottom) overview images stitched together from eight individual image pairs. While the whole samples is less than 50 nm thick, sample thickness below 20 nm was reached throughout the lower half of the specimen over several micrometers. The insert shows measured thickness of an EELS line scan from the area indicated by the white arrow. The MAADF image shows orientation contrast facilitating easy detection of grain boundaries. b) High magnification STEM HAADF of twin boundaries at a specimen thickness of 33 nm (center of the lamella). c, d) High magnification STEM HAADF of general grain boundaries at a specimen thickness of 19 nm and 10 nm, respectively.

detector (MAADF). The images were stitched together from eight pairs of images at maximum scan-width of the system. The HAADF signal (top) showed nearly pure mass/thickness contrast, but the MAADF, which collects scattered electrons of the angular range between 52 and 100 mrad, offered strong orientation contrast in addition to mass/thickness contrast. Provided the specimen has homogenous thickness, the MAADF can thus be easily used to identify general grain boundaries.

EELS thickness measurements showed that the lower half of the lamella has a specimen thickness between 10 and 20 nm throughout the whole length of the lamella (about 6 μm). It is empirically shown that a specimen thickness of 20 nm or below is necessary to detect unambiguously elemental changes of copper across random grain boundaries by EELS [44–46]. The top-most area of the $Cu(In,Ga)Se_2$ layer had an average thickness of 40 nm as measured by EELS (not shown). These areas were successfully used for atomically resolved chemical mapping of ordered grain boundaries and planar defects which do not have difficulties due to geometric projection. Fig. 8b shows the HAADF image of such a defect area at a specimen thickness of ∼32 nm. Fig. 8c and d show HAADF images of random grain boundaries at specimen thicknesses of 19 and 10 nm.

4. Conclusions

In this work, we showed that FIB sample preparation without additional preparation steps is capable of providing excellent samples suitable for state-of-the-art aberration corrected STEM microscopy, yielding atomic resolution images and EELS analysis even at low-voltages.

This was demonstrated on five different materials, with a total of nine prepared FIB lamellas all with an average thickness of 20–45 nm over an extensive area of several μm. All samples showed a sufficiently low amount of surface damage to allow clean atomic resolution HAADF z-contrast images at 100 and 60 kV. While careful adjustment of the milling steps was needed for each individual case, it could be shown that the technique is generally applicable for a broad range of very different materials and that the results are fully reproducible.

The thinnest specimen, a cross-section sample of a working thin film solar-cell device, showed regions with 10–20 nm thickness over a length of 6 μm, allowing elemental mapping across general grain boundaries without geometrical projection artefacts. Atomic resolution HAADF imaging of the thinnest areas could be performed with no apparent artefacts due to the FIB sample preparation.

The optimized preparation technique is based on the standard lift-out procedure and offers all the according advantages such as target preparation and the ability to prepare both cross-sections as well as plan-view samples. As shown for a YAG crystal, this enables for the first time investigations on specific sample areas which were previously impossible due to the lack of sufficiently thin and clean specimens.

Finally, a novel 'wedge pre-milling' step has been demonstrated. This prevents the loss of protective surface layers even during the final milling steps, enabling surface and close-to-the-surface features to be investigated without preparation damage.

In addition, parallel surfaces can be maintained even for very thin samples.

This work does not claim that FIB prepared samples are free of any preparation induced damage. A certain amount of Ga implementation and some structural damage, in particular at the sample surface, is always to be expected even at low-kV milling. However, for the samples in this study, these effects were not limiting.

Acknowledgments

References

[1] J. Orloff, M. Utlaut, L. Swanson, High Resolution Focused Ion Beams: FIB and its Applications, first ed., Kluwer Academic/Plenum Publishers, New York, 2003.

[2] L.A. Giannuzzi, F.A. Stevie, A review of focused ion beam milling techniques for TEM specimen preparation, Micron 30 (1999) 197–204.

[3] R.M. Langford, A.K. Petford-Long, Preparation of transmission electron microscopy cross-section specimens using focused ion beam milling, Journal of Vacuum Science and Technology A 19 (2000) 2186–2193.

[4] K. Ozasa, Y. Aoyagi, M. Iwaki, M. Hara, M. Maeda, Nanofabrication of cylindrical STEM specimen of InGaAs/GaAs quantum dots for 3D-STEM observation, Ultramicroscopy 101 (2004) 55–61.

[5] M.K. Miller, K.F. Russell, G.B. Thompson, R. Alvis, D.J. Larson, Review of Atom Probe FIB-based specimen preparation methods, Microscopy and Microanalysis 13 (2007) 428–436.

[6] M. Schaffer, J. Wagner, Block lift-out sample preparation for 3D experiments in a dual beam focused ion beam microscope, Microchimica Acta 161 (2007) 421–425.

[7] R.M. Langford, Y.Z. Huang, S. Lozano-Perez, J.M. Titchmarsh, A.K. Petford-Long, Preparation of site specific transmission electron microscopy plan-view specimens using a focused ion beam system, Journal of Vacuum Science and Technology 19 (2001) 755–758.

[8] M. Sugiyama, G. Sigesato, A review of focused ion beam technology and its applications in transmission electron microscopy, Journal of Electron Microscopy 53 (2004) 527–536.

[9] R. Anderson, S.J. Klepeis, Practical aspects of FIB TEM specimen preparation, in: L.A. Giannuzzi, F.A. Stevie (Eds.), Introduction to Focused Ion Beams, Springer Science+Business Media, New York, 2005, pp. 173–200.

[10] T. Kamino, T. Yaguchi, T. Hashimoto, T. Ohnishi, K. Umemura, A FIB micro-sampling technique and a site specific TEM specimen preparation method, in: L.A. Giannuzzi, F.A. Stevie (Eds.), Introduction to Focused Ion Beams, Springer Science+Business Media, New York, 2005, pp. 229–246.

[11] R.M. Langford, Focused ion beams techniques for nanomaterials characterization, Microscopy Research and Technique 69 (2006) 538–549.

[12] E. Montoya, S. Bals, M.D. Rossell, D. Schryvers, G. Van Tendeloo, Evaluation of top, angle, and side cleaned FIB samples for TEM analysis, Microscopy Research and Technique 70 (2007) 1060–1071.

[13] H.C. Floresca, J. Jeon, J.G. Wang, M.J. Kim, The focused ion beam fold-out: sample preparation method for transmission electron microscopy, Microscopy and Microanalysis 15 (2009) 558–563.

[14] M. Bosman, V.J. Keast, J.L. García-Muñoz, A.J. D'Alfonso, S.D. Findlay, L.J. Allen, Two-dimensional mapping of chemical information at atomic resolution, Physical Review Letters 99 (2007) 086102.

[15] K. Kimoto, T. Asaka, T. Nagai, M. Saito, Y. Matsui, K. Ishizuka, Element-selective imaging of atomic columns in a crystal using STEM and EELS, Nature 450 (2007) 702–704.

[16] D.A. Muller, L. Fitting Kourkoutis, M. Murfitt, J.H. Song, H.Y. Hwang, J. Silcox, N. Dellby, O.L. Krivanek, Atomic-scale chemical imaging of composition and bonding by aberration-corrected microscopy, Science 319 (2008) 1073–1076.

[17] G.A. Botton, S. Lazar, C. Dwyer, Elemental mapping at the atomic scale using low accelerating voltages, Ultramicroscopy 110 (2010) 926–934.

[18] M. Varela, M.P. Oxley, W. Luo, J. Tao, M. Watanabe, A.R. Lupini, S.T. Pantelides, S.J. Pennycook, Atomic-resolution imaging of oxidation states in manganites, Physical Review B 79 (2009) 085117.

[19] L.Q. Wang, B. Schaffer, A.J. Craven, I. MacLaren, S Miao, I.M. Reaney, Atomic scale structural and chemical quantification of non-stoichiometric defects in Ti and Bi doped BiFeO$_3$, Microscopy and Microanalysis 17 (Suppl. 2) (2011) 1896–1897.

[20] M. Arredondo, Q.M. Ramasse, M. Weyland, R. Mahjoub, I. Vrejoiu, D. Hesse, N.D. Browning, M. Alexe, P. Munroe, V. Nagarajan, Direct evidence for cation non-stoichiometry and Cottrell atmospheres around dislocation cores in functional oxide interfaces, Advanced Materials 22 (2010) 2430–2434.

[21] G. Yang, Q.M. Ramasse, R.F. Klie, Direct measurement of charge transfer in thermoelectric Ca$_3$Co$_4$O$_9$, Physical Review B 78/15 (2008) 153109.

[22] J.P McCaffrey, M.W. Phaneuf, L.D. Madsen, Surface damage formation during ion-beam thinning of samples for transmission electron microscopy, Ultramicroscopy 87 (2001) 97–104.

[23] J.M. Cairney, P.R. Munroe, Redeposition effects in transmission electron microscope specimens of FeAl-WC composites prepared using a focused ion beam, Micron 34 (2003) 97–107.

[24] T. Kamino, T. Yaguchi, Y. Kuroda, T. Ohnishi, T. Ishitani, Y. Miyahara, Z. Horita, Evaluation of TEM samples of an Mg–Al alloy prepared using FIB milling at the operating voltages of 10 kV and 40 kV, Journal of Electron Microscopy 53 (2004) 459–463.

[25] T. Ishitani, K. Umemura, T. Ohnishi, T. Yaguchi, T. Kamino, Improvements in performance of focused ion beam cross-sectioning: aspects of ion-sample interaction, Journal of Electron Microscopy 53 (2004) 443–449.

[26] N.I. Kato, Reducing focused ion beam damage to transmission electron microscopy samples, Journal of Electron Microscopy 53 (2004) 451–458.

[27] C.-M. Park, J.A. Bain, T.W. Clinton, P.A. van der Heijden, T.J. Klemmer, Measurement of Ga implantation profiles in the sidewall and bottom of focused-ion-beam-etched structures, Applied Physics Letters 84 (2004) 3331–3333.

[28] J.C. Reiner, P. Nellen, U. Sennhauser, Gallium artefacts on FIB-milled silicon samples, Microelectronics Reliability 44 (2004) 1583–1588.

[29] S. Rubanov, P.R. Munroe, FIB-induced damage in silicon, Journal of Microscopy 214 (2004) 213–221.

[30] Y. Yabuuchi, S. Tametou, T. Okano, S. Inazato, S. Sadayama, Y. Yamamoto, K. Iwasaki, Y. Sugiyama, A study of the damage on FIB-prepared TEM samples of Al$_x$Ga$_{1-x}$As, Journal of Electron Microscopy 53 (2004) 471–477.

[31] S. Rubanov, P.R. Munroe, Damage in III–V compounds during focused ion beam milling, Microscopy and Microanalysis 11 (2005) 446–455.

[32] Z. Wang, T. Kato, T. Hirayama, N. Kato, K. Sasaki, H. Saka, Surface damage induced by focused-ion-beam milling in a Si/Si p–n junction cross-sectional specimen, Applied Surface Science 241 (2005) 80–86.

[33] J. Yu, J. Liu, J. Zhang, J. Wu, TEM investigation of FIB induced damages in preparation of metal material TEM specimens by FIB, Materials Letters 60 (2006) 206–209.

[34] S. Kim, M. Jeong Park, N.P. Balsara, G. Liu, A.M. Minor, Minimization of focused ion beam damage in nanostructured polymer thin films, Ultramicroscopy 111 (2011) 191–199.

[35] P. Roediger, H.D. Wanzenboeck, S. Waid, G. Hochleitner, E. Bertagnolli, Focused-ion-beam-inflicted surface amorphization and gallium implantation-new insights and removal by focused-electron-beam-induced etching, Nanotechnology 22 (2011) 235302–235312.

[36] L.A. Giannuzzi, R. Geurts, J. Ringnalda, 2 keV Ga+FIB milling for reducing amorphous damage in silicon, Microscopy and Microanalysis 11 (2005) 828–829.

[37] M. Baram, W.D. Kaplan, Quantitative HRTEM analysis of FIB prepared specimens, Journal of Microscopy 232 (2008) 395–405.

[38] S. Bals, W. Tirry, R. Geurts, Z. Yang, D. Schryvers, High-quality sample preparation by low kV FIB thinning for analytical TEM measurements, Microscopy and Microanalysis 13 (2007) 80–86.

[39] R.M. Langford, M. Rogers, In situ lift-out: steps to improve yield and a comparison with other FIB TEM sample preparation techniques, Micron 39 (2008) 1325–1330.

[40] J.F. Ziegler, M.D. Ziegler, J.P. Biersack, SRIM—The Stopping and Range of Ions in Matter, SRIM Co., USA, 2010.

[41] FEI Company, xT Nova NanoLab User's Manual, 2003, first ed., pp. 5–57.

[42] S.M. Schwarz, B.W. Kempshall, L.A. Giannuzzi, M.R. McCartney, Avoiding the curtaining effect: backside milling by FIB INLO, Microscopy and Microanalysis 9 (Suppl. 2) (2003) 116–117.

[43] K. Marquardt, Q.M. Ramasse, C. Kisielowski, R. Wirth, Insight into the effective grain boundary width for diffusion, American Mineralogist 96 (2011) 1521–1529.

[44] B. Schaffer, D. Abou-Ras, S.S. Schmidt, M. Schaffer, R. Caballero, High-Resolution EELS Characterization of Grain Boundaries in Cu(In,Ga)Se$_2$, 2011, MSM XVII Abstract, p. 23.

[45] B. Schaffer, F. Azough, D. Abou-Ras, S.S. Schmidt, M Schaffer, M Sarahan, Q. Ramasse, R. Caballero, Applications of atomic-resolution EELS mapping at low kV, Microscopy and Microanalysis 17 (Suppl. 2) (2011) 786–787.

[46] D. Abou-Ras, B. Schaffer, M. Schaffer, S.S. Schmidt, R. Caballero, T. Unold, Direct insight into grain boundary reconstruction in polycrystalline Cu(In,Ga)Se$_2$ with atomic resolution, Physical Review Letters, in press.